Dissociation Dynamics of Sequential Ionic Reactions: Heats of Formation of Tri-, Di-, and Monoethylphosphine

James P. Kercher,[†] Zsolt Gengeliczki,[‡] Bálint Sztáray,[‡] and Tomas Baer*,[†]

The Department of Chemistry, The University of North Carolina at Chapel Hill, Chapel Hill, North Carolina, 27599-3290, and The Institute of Chemistry, Eötvös Loránd University, 1/A Pázmány Péter stny. Budapest 1117, Hungary

Received: August 14, 2006; In Final Form: September 28, 2006

The sequential ethene (C_2H_4) loss channels of energy-selected ethylphosphine ions have been studied using threshold photoelectron photoion coincidence (TPEPICO) spectroscopy in which ion time-of-flight (TOF) distributions are recorded as a function of the photon energy. The ion TOF distributions and breakdown diagrams have been modeled in terms of the statistical RRKM theory for unimolecular reactions, providing 0 K dissociation onsets, E_0, for the ethene loss channels. Three RRKM curves were used to model the five measurements, since two of the reactions differ only by the internal energy of the parent ion. This series of dissociations provides a detailed check of the calculation of the product energy distribution for sequential reactions. From the determined E_0's, the heats of formation of several ethylphosphine neutrals and ions have been determined: $\Delta_f H°_{298K}[P(C_2H_5)_3] = -152.7 \pm 2.8$ kJ/mol, $\Delta_f H°_{298K}[P(C_2H_5)_3^+] = 571.6 \pm 4.0$ kJ/mol, $\Delta_f H°_{298K}[HP(C_2H_5)_2] = -89.6 \pm 2.1$ kJ/mol, $\Delta_f H°_{298K}[HP(C_2H_5)_2^+] = 669.9 \pm 2.5$ kJ/mol, $\Delta_f H°_{298K}[H_2PC_2H_5] = -36.5 \pm 1.5$ kJ/mol, $\Delta_f H°_{298K}[H_2PC_2H_5^+] = 784.0 \pm 1.9$ kJ/mol. These values have been supported by G2 and G3 calculations using isodesmic reactions. Coupled cluster calculations have been used to show that the C_2H_4 loss channel, which involves a hydrogen transfer step, proceeds without a reverse energy barrier.

Introduction

A cursory literature search for alkylphosphines reveals a decided dearth of quantitative studies aimed at their physical properties.[1−6] The major interest in alkylphosphines is as ligands in organometallic catalysis, where the electron donating power of the phosphorus lone pair electrons results in strong metal−phosphine interactions.[6,7] This interaction can have profound effects on the catalytic activity, influencing selectivity[7,8] and the reaction rate[2]. Indeed, it is our prior investigation of the tricarbonylnitrosyl derivatives ($Co(CO)_2NOPR_3$),[6] where R can be CH_3, C_2H_5, etc., that has led us to investigate the physical properties such as heats of formation, ionization energies, and bond dissociation energies of the alkylphosphine series. This started with trimethylphosphine[9] and is continuing here with the ethylphosphines, $H_nP(C_2H_5)_{3-n}$, where $n = 0-2$.

A thorough investigation of the phosphine literature reveals a surprising lack of established and reliable thermochemical information about this simple and important series of molecules. For example, the neutral $P(C_2H_5)_3$ heat of formation varies wildly from −225 kJ/mol found in the GIANT compilation of Lias et al.[10] to −150 kJ/mol listed in Cox and Pilcher's compilation.[11] No reference at all can be found for the monoethylphosphine heat of formation. Even the methylphosphine heats of formation are limited. The one exception to all this is phosphine, PH_3, whose heat of formation is known to within 2 kJ/mol. While preparing this paper, a series of high-level calculations dealing with the thermochemistry of organophosphorus(III) compounds was published by Dorofeeva and Moiseeva.[12] Specifically, they determine a new value of −150.0 kJ/mol for $P(C_2H_5)_3$ using isodesmic reactions. Additionally, group additivity values were also determined, which yield neutral heats of formation of −88.4 and −36.0 kJ/mol for $HP(C_2H_5)_2$ and $H_2P(C_2H_5)$, respectively.

One goal in this paper is the experimental determination of the thermochemistry of the ethylphosphine series, $H_nP(C_2H_5)_{3-n}$ for $n = 0-2$, by measuring the energetics of the sequential ethene loss channels using dissociative photoionization and relating it to the reaction thermochemistry of $AB \rightarrow A + B$, in which

$$E_0 = \Delta_f H°_{0K}[A^+] + \Delta_f H°_{0K}[^\bullet B] - \Delta_f H°_{0K}[AB] \quad (1)$$

If the dissociation energy, E_0, can be measured and two of the three heats of formation are known, the third can be determined. However, the measurement of the dissociation energy is not always straightforward. Factors such as the internal energy distribution[13−15] of the starting neutral species, a reverse energy barrier[9] in the dissociation, slow dissociation rate constants, and isomerization[9,16−22] often complicate this determination.

In addition to the lowest energy dissociation channel, ions can fragment via parallel or sequential pathways at higher energies. For parallel reactions, the appearance of the second pathway is shifted to higher energy as a result of the competitive shift.[23−25] This is because, at the dissociation limit for the second channel, the rate of the lowest energy pathway can be orders of magnitude higher than the rate of the second pathway, preventing the observation of products at the dissociation limit. Ions may also dissociate in a stepwise or sequential manner at higher energy, such as $ABC^+ \rightarrow AB^+ + C \rightarrow A^+ + B + C$. In this case, the internal energy of the molecular ion, ABC^+, is partitioned between the fragment ion, AB^+, and neutral C ligand upon the first dissociation. As a result, ion AB^+ has a much broader internal energy distribution which is reflected in the appearance of the final ion, A^+. We have recently shown[13,26]

[†] The University of North Carolina at Chapel Hill.
[‡] Eötvös Loránd University.

10.1021/jp0652392 CCC: $37.00
Published on Web 12/14/2006

that the threshold photoelectron photoion coincidence (TPEPICO) modeling software can model both competitive and sequential dissociation pathways accurately.

In the case of slowly dissociating ions, the observed fragment ion onset is shifted to energies above the true dissociation limit by the so-called kinetic shift[13,23,24,27−29] because the ions do not have time to dissociate during mass analysis. Experiments that simply measure the ion yield as a function of the ionizing energy are not sensitive to the effects of a kinetic shift, which is the case for two electron impact studies on the alkylphosphine ions by Wada and Kiser[3] and Bogolyubov et al.[4] The TPEPICO experiment, on the other hand, is well-suited to study the effects of slowly dissociating ions. The time-of-flight (TOF) distributions recorded in the TPEPICO experiment can be modeled in terms of the statistical RRKM theory,[9,13,30,31] and a unique $k(E)$ curve can be obtained by fitting several TOF distributions at various ion internal energies. The measured rate curve can then be extrapolated to the dissociation threshold, thus accounting for the kinetic shift.[6,13]

An additional advantage of measuring the dissociation rate constant is in establishing the absence of a reverse barrier. If the transition state is loose (no reverse barrier), the entropy of activation will be positive. This is an important issue in these reactions which dissociate via a rearrangement rather than a simple bond-breaking step.

The dissociations of the three ethylphosphine ions proceed primarily via sequential ethene loss channels, along with a minor methyl loss channel in the case of triethylphosphine, as described below:

$$\xrightarrow{E_0(1p)_T} H_2C{=}P(C_2H_5)_2^+ + CH_3 \qquad (2p)$$

$$P(C_2H_5)_3 + h\nu \xrightarrow{E_0(1)_T} HP(C_2H_5)_2^+ + C_2H_4 \xrightarrow{E_0(2)_T} H_2PC_2H_5^+ + 2C_2H_4 \xrightarrow{E_0(3)_T} PH_3^+ + 3C_2H_4 \qquad (2)$$

$$HP(C_2H_5)_2^+ + h\nu \xrightarrow{E_0(2)_D} H_2PC_2H_5^+ + C_2H_4 \xrightarrow{E_0(3)_D} PH_3^+ + 2C_2H_4 \qquad (3)$$

$$H_2PC_2H_5^+ + h\nu \xrightarrow{E_0(3)_M} PH_3^+ + C_2H_4 \qquad (4)$$

where equations (2) are for triethyl-, (3) for diethyl-, and (4) for monoethylphosphine. (Reaction 2p is the parallel step.) The E_0's are the 0 K energy differences between the neutral starting molecule and the indicated products, and the subscripts indicate whether the reaction is for the triethyl-, diethyl-, or monoethylphosphine. In this series, the first C_2H_4 loss channel in $HP(C_2H_5)_2$ (eq 3) is the same reaction as the second C_2H_4 loss in $P(C_2H_5)_3$ (eq 2), and therefore they must be modeled using the same $k(E)$ curve. The only difference between these two dissociations is the internal energy of the $HP(C_2H_5)_2^+$. Similarly, the second dissociation in $HP(C_2H_5)_2$ is identical to the C_2H_4 loss in $H_2P(C_2H_5)$, so the same $k(E)$ curve is applied to both of those reactions. All in all, the five experimental measurements are modeled with three $k(E)$ curves. This redundancy will provide a valuable check on the calculation of the energy partitioning between the daughter ion and neutral fragment, which has been used extensively in modeling higher energy dissociations[14,15]

By determining the three dissociation onsets, the thermochemistry for these six species (three neutral precursors and the corresponding molecular ions) can be determined. The previous work of Wada and Kiser[3] as well as Bogolyubov et al.[4] not only suffered from the poor resolution of their electron impact experiment, no correction for the kinetic shift, but also a reliance on estimated heats of formation of the neutral precursor. In our study, the series is anchored to the well-known PH_3^+ heat of formation and the accurately established neutral C_2H_4 heat of formation, these being the two of three known heats of formation needed in the thermochemical energy relation (eq 1).

Experimental Approach

Threshold Photoelectron Photoion Coincidence. The TPEPICO apparatus has been described in detail elsewhere.[9,32−35] Briefly, room-temperature sample vapor is introduced into the ionization region through a small stainless steel capillary and ionized with vacuum ultraviolet (vacuum-UV) light (tunable from 7 to 14 eV) from a hydrogen discharge lamp dispersed by a 1 m normal incidence monochromator with a resolution of 9 meV at a photon energy of 10.0 eV. The vacuum-UV wavelengths are calibrated by using the Lyman-α and -β emissions at 1215.67 and 1025.72 Å, respectively, which are intense lines in the hydrogen lamp spectrum. The ions and electrons are extracted in opposite directions with an electric field of 20 V/cm. Electrons pass through a second acceleration region where they reach a final energy of 74 eV in the 13 cm long drift region. The applied voltages are designed to velocity focus threshold electrons onto a 1.4 mm aperture at the end of the electron drift region, where a Channeltron detects them. At the same time, energetic electrons focused to concentric rings around the central hole are collected by a second Channeltron after they pass through a 3 × 5 mm opening located close to the central 1.4 mm hole. This provides a measure of the hot electron signal which contaminates the threshold signal.[35]

Reflecting TOF Mass Spectrometer Used for Triethyl Phosphine. The reflecting time-of-flight (ReTOF) system consists of single acceleration and deceleration fields, in which the ions are accelerated to 100 eV in the first 5 cm long acceleration region and travel 40 cm in the first drift region. The ions are then reflected and travel through another 35 cm second drift region before being collected by a tandem multichannel plate ion detector. Ions that dissociate in the first drift region do not penetrate as deeply into the reflectron as parent ions and are thus separated from the parent ions. The drift peak appears as a sharp, symmetric peak just after the corresponding metastable daughter ion peak.

Linear TOF Mass Spectrometer Used for Di- and Monoethylphosphine. In the LinTOF, ions are accelerated to 100 eV in the first 5 cm long acceleration region and to 280 eV in a short second acceleration region after which they travel 40 cm in the first drift region. The ions are then decelerated and travel through a 7.5 cm second drift region before being collected by a tandem multichannel plate ion detector. The deceleration serves to separate ions which have dissociated in the first drift region from ions which do not dissociate. The drift peak appears as a broad peak at a higher TOF than the parent ion.

The main advantage of the ReTOF mass spectrometer is its mass resolution, which would be important in this series if there were a dominant ethyl (C_2H_5) loss channel in addition to the primary ethene (C_2H_4) loss channel. However, no ethyl loss channel was observed in triethylphosphine. The main disadvantage of the ReTOF is for the case when a parent ion loses a massive neutral fragment, such as the ethene loss (m/z 24) from monoethylphosphine (m/z 62). The fragment ions produced during the course of acceleration, or in the first drift region, lose so much kinetic energy as a result of their mass loss that

they are no longer efficiently reflected in the ReTOF and are consequently lost. We estimate that if ions lose more than 25% of their kinetic energy, the daughter ion loss becomes significant.[13] This is the case for both di- and monoethylphosphines, for which the neutral fragment is 40% of the ion mass (second step in diethylphosphine). As a result, several of the experiments were carried out in both the ReTOF and the LinTOF systems. In either case, the electron and ion signals are used as start and stop pulses for measuring the ion TOF. A single TPEPICO TOF spectrum could be collected in 2−5 h.

Subtraction of Energetic Electron Contamination. The primary TPEPICO experimental data consist of ion TOF distributions at various photon energies. From these we can construct a breakdown diagram, which is the fractional abundance of parent and the various daughter ions as a function of the photon energy. In addition, we analyze the shape of the ion TOF distributions at photon energies where the dissociation rate constants are in the range of 10^3-10^7 s^{-1}. The subtraction of the hot electron signal for the breakdown diagram as described by Fogleman et al.[32] involves subtracting a fraction of the TOF peak areas in the hot TPEPICO signal from those in the threshold TPEPICO TOF data. The corrected peak areas are then given by

$$T_n = C_n - FR_n \quad (5)$$

where T_n is the true threshold integrated area of ion n and C_n and R_n represent the integrated areas of ion n, in the center and ring TOF spectra, respectively. The factor F is a constant factor determined by the ratio of center parent ion peak area to the ring parent ion peak area in a TOF distribution well above the dissociation limit. At these high energies, the parent ion signal in the center TOF spectrum should be zero, and any nonzero area is due solely to hot electron contamination.

For the TOF distributions, the asymmetric peak shape must be conserved, and therefore a point-by-point subtraction is employed. Because the two spectra have been recorded using two different time to pulse height converters, a second-order fitting algorithm is used to align the spectra before the subtraction. The spectra are then subtracted point by point using a cubic spline algorithm. The same factor is used as in the breakdown diagram.

Both triethyl- and diethylphosphine were acquired from Strem chemicals and used without further purification. Monoethylphosphine is not commercially available, and the synthesis is described below.

Photoelectron Spectroscopy. *Threshold Photoelectron Spectroscopy (TPES).* Threshold and hot electrons were collected by scanning the monochromator at a rate of 0.5 Å/min while collecting electron signals from both the center and off-center detectors. The electron signals were then normalized by the photon intensity, monitored by a photomultiplier tube. The true threshold spectrum was obtained by subtracting a fraction of the off-center signal from the center signal, using the same factor that is applied to the TOF distributions and breakdown curve.

Ultraviolet Photoelectron Spectroscopy. The ultraviolet photoelectron spectroscopy (UPS) instrument was an ATOMKI ESA 32, which has been described in detail elsewhere[36] Briefly, the instrument is equipped with a Leybold-Heraeus UVS 10/35 high-intensity gas discharge photon source. The UPS spectrum is obtained by ionizing the neutral precursor using the 21.217 eV He(I) line and scanning the energy of the ejected photoelectrons. Electrons were collected using a hemispherical energy analyzer, which has a resolution on the order of 20 meV. The spectrum was calibrated using the CO_2 $^2\Pi_g$ peak at 13.777 eV.

Theoretical Methodology. *Modeling.* The data analysis, including RRKM rate constant calculations, requires knowledge of the vibrational frequencies of the starting molecules and the molecular ions, as well as the various transition states. Because the reactions are sequential, the daughter ion and neutral ligand vibrational frequencies are also needed for the calculation of the product energy distribution. All of these calculations were carried out using the Gaussian 03 program suite[37] provided by the ITS Research computing facility at the University of North Carolina at Chapel Hill. The geometry and vibrational frequencies of all molecules studied were calculated using the Becke three-parameter exchange functional,[38] the electron correlation functional of Lee−Yang−Parr (B3LYP)[39] with the 6-311+G** basis set and are listed in Table 2. No scale factor was applied to the vibrational frequencies of the stable species. The transition states were determined by the QST3 method,[40] using the same level of theory and basis set. This provides a starting set of frequencies for modeling the data. The four lowest frequencies in the transition state are treated as adjustable parameters, as described below.

Ionization Energies. The adiabatic ionization energies were calculated at the B3LYP/6-311+G**, G3,[41] and CBSQB3[42] levels of theory and the vertical ionization energies at the B3LYP/6-311+G** level of theory for the three neutral precursors. The vertical ionization energy was determined by fixing the geometry at the optimized structure of the neutral and removing one electron. The adiabatic and vertical ionization energies are then given by the difference between the ion and neutral total energies. We have also calculated the adiabatic ionization energies at the B3LYP/6-311+G**, G3, CBSQB3, and W1U levels of theory for PH_3. This is to ensure the thermochemistry is anchored to an accurate PH_3^+ heat of formation. These results are summarized in Table 1.

Thermochemistry. Calculations were carried out using the G2 and G3 methods as described by Curtiss and co-workers.[41,43−45] These were used in three isodesmic reactions to support the derived thermochemistry of the neutral alkylphosphines. These results are summarized in Table 4.

Potential Energy Surfaces. Several key species along the reaction coordinates for ethene loss from all three molecular ions were calculated at the B3LYP/6-311+G** level of theory. This was used to piece together approximate potential energy curves for these reactions. Additionally, single-point coupled-cluster[46] calculations with perturbative triplet excitations, CCSD(T), were carried out for the monomethylphosphine using the cc-pVTZ basis set at the B3LYP/6-311+G** optimized geometries of the molecular ion, transition state, and products for this reaction as well. This was used to address the issue of reverse energy barriers associated with the hydrogen-transfer dissociations, which would affect the derived heats of formation. Unfortunately, the coupled-cluster calculations on the transition states for tri- and diethylphosphine did not converge, so we only present the monoethylphosphine results.

Synthesis of Monoethylphosphine. The synthesis of monoethylphosphine was carried out as described by Van Hooijdonk et al.[47] A 500 mL three-necked round-bottomed flask was equipped with a vacuum/nitrogen inlet, a thermometer, and a magnetic stir bar. With a vigorous flow of nitrogen, 6.9 g of freshly cut Na (0.1 g pieces) was added to 180 mL of diethene glycol diethyl ether (ethyl diglyme), followed by 4.7 g of naphthalene. After a few minutes, a slurry of 3.1 g of red

TABLE 1: Comparison of Experimental and Calculated Ionization Energies[a]

	adiabatic ionization energies					vertical ionization energies	
species	experiment	DFT[f,g]	G3[f,h]	CBSQB3[f,h]	W1U[f,h]	experiment	DFT[f−h]
PH_3	9.870 ± 0.002[b]	9.80	9.87	9.86	9.882	10.59 ± 0.05[b]	10.54
$H_2P(C_2H_5)$	8.80 ± 0.06[c]	8.79	8.91	8.87	−	9.50 ± 0.035[c]	9.41
	8.50 ± 0.02[d]						
$HP(C_2H_5)_2$	7.87 ± 0.02[d]	8.03	8.17	8.14	−	−	8.68
$P(C_2H_5)_3$	7.50 ± 0.03[d]	7.47	7.64	7.66	−	8.25 ± 0.03[c]	8.14
	7.50 ± 0.03[e]						

[a] All values in electronvolts. [b] Berkowitz et al.[49] [c] UPS measurement in this study. [d] TPEPICO result from this study. [e] Gengelizcki et al.[6] [f] Calculated using the Gaussian 03 software suite.[37] [g] B3LYP/6-311++G**. [h] Calculations from this study.

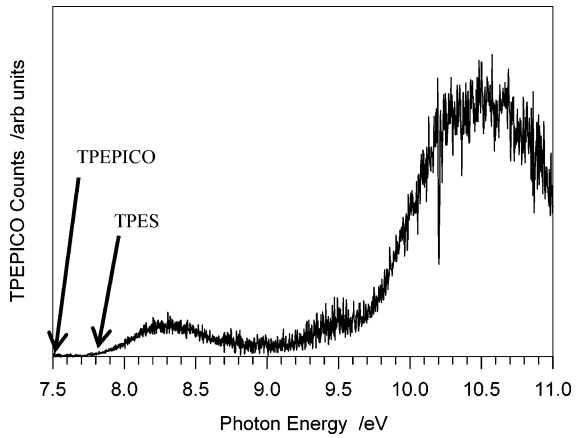

Figure 1. Threshold photoelectron spectrum (TPES) of triethylphosphine from 7.5 to 11.0 eV. The TPES arrow (7.80 eV) is the adiabatic ionization energy determined from this spectrum, while the TPEPICO arrow (7.50 eV) is the adiabatic ionization energy determined from modeling the TPEPICO data sets. The difference is 300 meV.

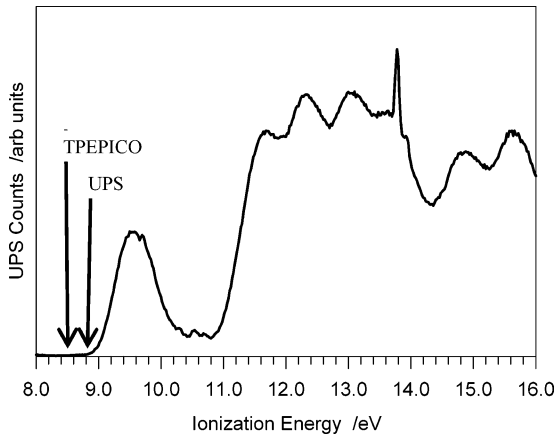

Figure 2. Ultraviolet photoelectron spectrum (UPS) of monoethylphosphine from 8.0 to 16.0 eV. The UPS arrow (8.80 eV) is the adiabatic ionization energy determined from the UPS spectrum, while the TPEPICO arrow (8.50 eV) is the adiabatic ionization energy obtained from modeling the TPEPICO data sets. The difference is 300 meV.

phosphorus and 10 mL of ethyl diglyme was added. The solution was brought to 50 °C and allowed to stir for 4 h. The slurry was cooled to −5 °C, and 14.8 g of *t*-BuOH in 30 mL of ethyl diglyme was added through a dropping funnel over a 20 min period. The solution was then stirred for another hour. A Vigreux column and condenser were added to the top of the flask in preparation of the addition of alkyl halide. A dry ice/acetone bath was used as 7.5 mL of ethyl bromide was added. The solution was stirred for 2 h, and the product was collected via vacuum distillation. This procedure yielded 25 g of monoethylphosphine.

Results

Determination of the Ionization Energies. The TPES of triethylphosphine, shown in Figure 1, exhibits a broad first band, which indicates that the ion and neutral geometries are very different, resulting in a broad Franck−Condon envelope. This situation is reminiscent of both NH_3 and PH_3, making the determination of the adiabatic ionization energy difficult. From the TPES we estimate that the upper limit to the adiabatic ionization energy is 7.80 ± 0.050 eV; however, the analysis of the TPEPICO data yields an adiabatic ionization energy of 7.50 ± 0.01 eV, which will be discussed in the TPEPICO results section. The vertical ionization energy of 8.25 ± 0.030 eV is much more easily established since it corresponds to the maximum in the TPES. The calculated vertical ionization energy, at the DFT level, is 8.14 eV which is almost within the measurement error. The calculated adiabatic ionization energies at the DFT, G3, and CBS-QB3 levels of theory are 7.47, 7.64, and 7.66 eV, respectively. These tend to favor the TPEPICO determination of 7.50 eV, although the agreement is not as good as one might hope for. The ionization energies are summarized in Table 1.

The UPS of monoethyl phosphine is shown in Figure 2. The vertical ionization energy was established to be 9.50 ± 0.035 eV, and an adiabatic ionization energy was estimated to be 8.80 ± 0.06 eV. As in the $P(C_2H_5)_3$ case, the adiabatic ionization is most likely lower than this value. An adiabatic ionization energy of 8.50 ± 0.01 eV was determined from this TPEPICO analysis, which will be addressed in Discussion. Calculations at the DFT, G3, and CBSQB3 levels of theory yield adiabatic ionization energies of 8.79, 8.91, and 8.87 eV. The agreement here certainly favors the TPES result over the TPEPICO result, unlike the triethylphosphine case. The calculated vertical ionization energy at the DFT level is 9.41 eV, a value in good agreement with the experimentally determined one. These values are also summarized in Table 1.

TPEPICO Results and Their Analysis. *Triethylphosphine.* The breakdown diagram of $P(C_2H_5)_3$ is given in Figure 3, and selected TOF distributions are presented in Figure 4. In the breakdown diagram, the points are the experimentally determined ion ratios and the solid lines are the simulated ion ratios. At low energies, only the parent ion is present (squares). At 9.25 eV, the first C_2H_4 loss channel appears, producing the diethylphosphine ion, $HP(C_2H_5)_2^+$ (triangles). The TOF distributions at 9.83 and 9.98 eV show these two ions, with the points representing the experimental TOF distribution and the solid lines representing the fit. The $P(C_2H_5)_3^+$ is observed as a sharp peak at 116 μs, and the $HP(C_2H_5)_2^+$ is observed over the entire region from 101 to 115 μs. The asymmetric peak from 101 to 104 μs is attributed to product ions resulting from parent ion

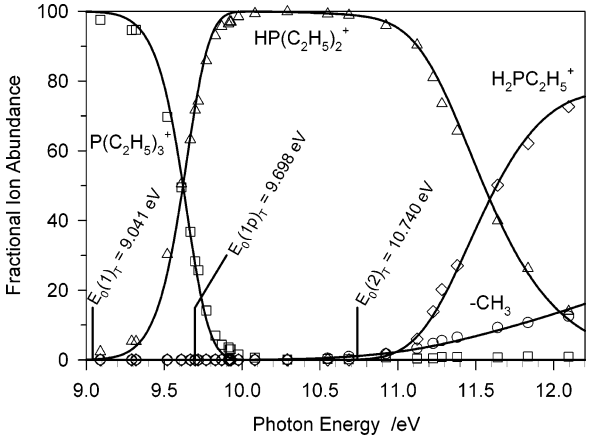

Figure 3. Breakdown diagram of triethylphosphine from 9.0 to 12.5 eV. The open points are the experimentally determined fractional ion abundances, and the solid lines are the fit.

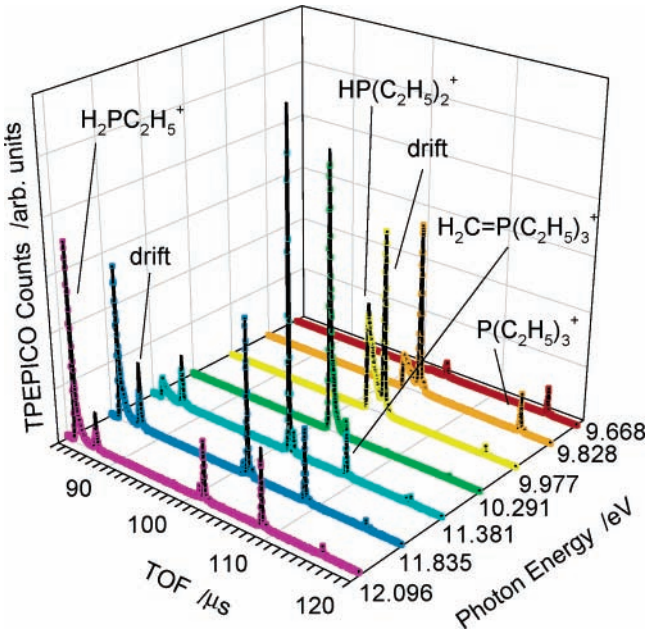

Figure 4. Selected time-of-flight (TOF) distributions for triethylphosphine using the reflecting TOF mass spectrometer. The points are experimental TOF distributions, and the solid lines are the fit.

dissociation in the acceleration region. The sharp peak at 105 μs is the drift peak, associated with product ions that are born in the drift region before being reflected. Any ions that dissociate in the reflectron are observed from 105 to 115 μs. Because their numbers are small and because they are spread out over many channels, we do not obtain any rate information from them. Ions that dissociate in the second drift region are observed at 116 μs along with any stable parent ions.

Because the dissociation is slow, the onset cannot be determined by the disappearance of the parent ion in the breakdown diagram.[9,13] This first dissociation step must be modeled by taking into account the RRKM dissociation rate constant, $k(E)$, shown in eq 6 in which E and E_0 are the ion energy and the activation energy measured from the ground state of the ion, σ is the reaction symmetry number, and $\rho(E)$ and $N^{\mp}(E-E_0)$ are the density of states of the ion and sum of states of the transition state, respectively.

$$k(E) = \frac{\sigma N^{\mp}(E - E_0)}{h\rho(E)} \qquad (6)$$

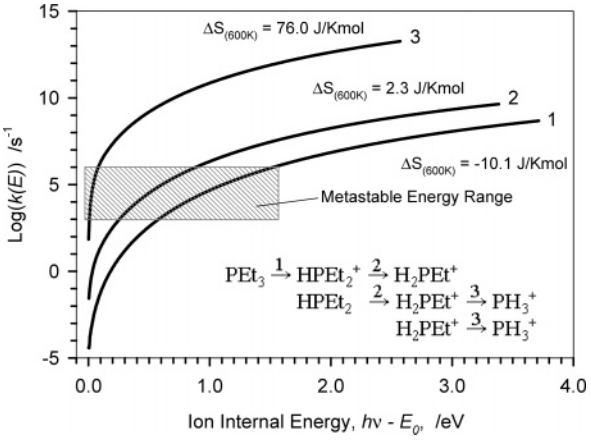

Figure 5. RRKM rate curves as a function of excess ion internal energy for the three ethene loss channels used in modeling all five experimental measurements. The gray area is the range in which the daughter ions are metastable, which yields direct kinetic information.

Because the ions are produced in a distribution of internal energies, $P(E)$, given by the room-temperature sample, we need to take this distribution of energies into account when modeling the data with the microcanonical rates of eq 6. The $P(E)$ function is given by eq 7 in which E is the neutral molar energy and T the sample temperature of 298 K.

$$P(E) = \frac{\rho(E)e^{-E/RT}}{\int_0^{\infty} \rho(E)\, e^{-E/RT} dE} \qquad (7)$$

Because slowly dissociating ions fragment during the course of their flight to the ion detector, the rate constants can be extracted from the analysis of the asymmetric daughter ion peak shape.[9,13] The $k(E)$ function (eq 6) was calculated with a density of states fixed by the calculated ion vibrational frequencies, adjusting only the 0 K dissociation threshold, E_0, and transition-state transitional vibrational frequencies. There are five transitional frequencies (See Table 2), which change during the course of reaction from vibrations to rotations of the products. We simply multiply these frequencies by a common factor until the data are best fitted. Simultaneously fitting the experimental TOF distributions at various photon energies and the breakdown diagram, by varying the above-mentioned parameters, yields a $k(E)$ function (shown in Figure 5, curve 1), and a dissociation onset, $E_0(1)_T$, of 9.041 $\pm$ 0.014 eV, where the 1 refers to the first C_2H_4 loss and the T to triethylphosphine. Although this first onset requires two adjustable parameters, the flexibility is limited by the simultaneous fitting of the TOF distributions and breakdown diagram.

The TOF distribution at 10.29 eV shows only the $HP(C_2H_5)_2^+$ peak. Although still asymmetric, the peak is much narrower than in the previous TOF distributions because of the increasing rate constant with increasing energy. At higher energy, the competitive CH_3 loss channel is observed as the sharp, symmetric peak at 108.8 μs in the TOF distributions. The $HP(C_2H_5)_2^+$ (104.5 μs) is also symmetric at this energy, indicating that $k(E)$ is now greater than 5×10^6 s^{-1}. The relative abundance of the CH_3 loss ion is given in the breakdown diagram (circles). Because this reaction is in competition with the low-energy C_2H_4 loss reaction, the appearance is shifted to higher energy by the so-called competitive shift. The fitting of this onset requires adjusting two parameters, the E_0 and transition state vibrational frequencies of the CH_3 loss channel. The latter parameter is adjusted to match the relative rates of the two reactions. How

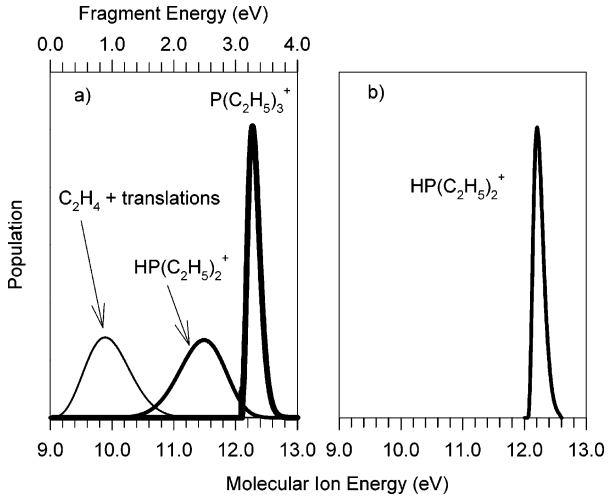

Figure 6. Internal energy distributions for the energy selected diethylphosphine ion (b) compared to the broadened diethylphosphine energy distribution as a result of the energy partitioning (a). The molecular ion energy relative to the neutral ground state is given on the lower axis, while the daughter ion and neutral product energies referenced to their ground states are shown on the upper axis.

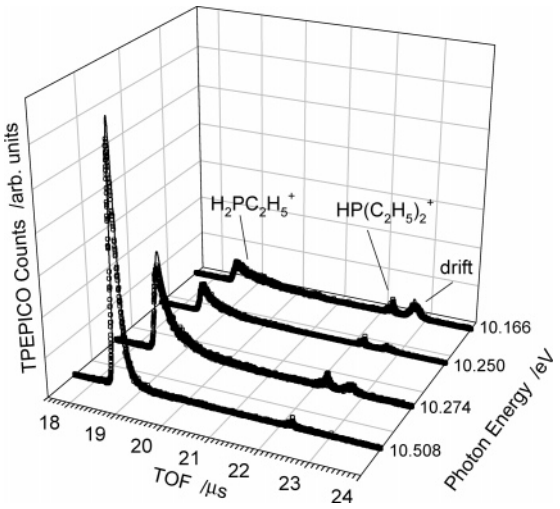

Figure 7. Selected time-of-flight (TOF) distributions for the diethylphosphine ion recorded using the linear TOF mass spectrometer. The points are experimental TOF distributions, and the solid lines are the fit.

quickly the CH_3 loss reaction catches up to the C_2H_4 loss reaction is a function of the transition-state vibrational frequencies. This results in a dissociation onset, $E_0(1p)_T$ (p for the parallel step) of 9.698 ± 0.022 eV for the CH_3 loss channel, which is almost 1.5 eV below the appearance of the ion in the breakdown curve.

The sequential C_2H_4 loss channel (diamonds in the breakdown diagram), producing the monoethyl phosphine ion, $H_2PC_2H_5^+$, is observed in the three high-energy TOF distributions of Figure 4. The dissociation is slow, so the ion appears from 84 to 100 μs in the TOF distributions, with the asymmetric part from 84 to 87.5 μs, the drift peak at 87.5 μs, and the reflectron dissociation from 87.5 to 100 μs. Because this is a sequential reaction, the $H_2P(C_2H_5)^+$ is produced from the $HP(C_2H_5)_2^+$, so the modeling involves calculating the product energy distribution between $HP(C_2H_5)_2^+$ and the neutral C_2H_4 ligand.[14] According to the statistical theory of energy partitioning, this distribution is given by $P(E_{ion}) = \rho_{ion}(E_{ion})\ \rho_{neutral}(E-E_{ion})$, where ρ_{ion} is the rovibrational density of states of the product ion, $\rho_{neutral}$ is the rovibrational density of states of the neutral convoluted with the translational density of states associated with the relative translational energy of the ion and neutral fragments, and E is the total energy above the dissociation threshold. $HP(C_2H_5)_2^+$ has a much broader internal energy distribution than its parent ion did, as illustrated in Figure 6. The narrow $P(C_2H_5)_3^+$ energy distribution, with a width of about 220 meV, is a result of the thermal energy distribution for this room-temperature sample selection, with the TPEPICO energy resolution contributing a negligible amount.

The consequence of the broadened internal energy distribution of the $HP(C_2H_5)^+$ ion is a much broader onset of the $H_2P(C_2H_5)_2^+$ ion signal in Figure 3. Because the only input in calculating the $HP(C_2H_5)_2^+$ energy distribution is the product vibrational frequencies, we have no adjustable parameters for fitting the slopes at the crossover energy. The excellent fit is simply a demonstration of how well the statistical theory predicts the energy partitioning in the dissociation of a polyatomic ion. E_0 and transition-state vibrational frequencies are adjusted to determine the unique $k(E)$ curve to fit the TOF distributions and breakdown curve, yielding a dissociation onset, $E_0(2)_T$, of 10.740 ± 0.024 eV. The calculated $k(E)$ curve (2) is shown in Figure 5. With the determination of this onset, the energy difference between $HP(C_2H_5)_2^+$ and $H_2PC_2H_5^+$ is established to be 1.70 ± 0.027 eV.

The final onset, $E_0(3)_T$, for the production of PH_3^+ could not be measured because the dissociation was too slow in the energy range of the TPEPICO experiment.

The above dissociation energies were determined with the assumed triethylphosphine ionization energy (IE) of 7.50 eV. This enters into the modeling because the dissociation rate constant is affected by the activation energy. For instance, if the assumed IE were reduced, the calculated rate constant would be lowered because of the increased E_0. But, this can be compensated for by raising the TS vibrational frequencies so that the $k(E)$ curve remains approximately constant, but with a change in slope. Because all three $k(E)$ curves can be adjusted in this way, the experimental data were fit with several assumed $P(C_2H_5)_3$ ionization energies. The best fit to all three data sets (the TOF distributions and breakdown curves for tri-, di-, and monoethylphosphines) is with a triethylphosphine ionization energy of 7.50 ± 0.01 eV.

The activation entropies obtained from the modeling provide valuable insight into the dissociation dynamics. The activation entropies calculated at 600 K are ($\Delta S^{\ddagger}_{600K}$) are −10.1 and 2.3 J K^{-1} mol^{-1} for the first and second ethene loss channels, respectively. These activation entropies are indicative of tight transition states, such as those involving a hydrogen transfer. On the other hand, the $\Delta S^{\ddagger}_{600K}$ for the methyl loss channel is 23.5 J/(K^{-1} mol^{-1}), indicating a loose transition state associated with homolytic bond cleavage. These entropies will be considered in more detail in the discussion.

Diethyl Phosphine. The TOF distributions for diethylphosphine are given in Figure 7. Because the parent ion loses 40% of its mass upon dissociation (in the second step), this experiment was done on the linear TOF mass spectrometer so that the appearance of the TOF distributions is different. Not only are the total time-of-flights much shorter, but also the drift peak appears at 22.7 μs, a longer TOF than the parent ion. This is because of the deceleration after the first drift region, as explained earlier in the Experimental Section. The parent ion is observed at 22.3 μs and the asymmetric daughter ion from 18.2 to 20.0 μs. The breakdown diagram data (open points) and simulated ion abundances (solid lines) are presented in Figure 8.

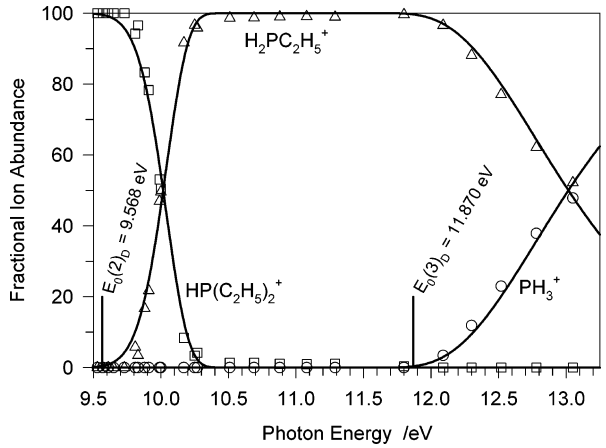

Figure 8. Breakdown diagram for diethylphosphine from 9.5 to 13.5 eV. The open points are the experimentally determined fractional ion abundances, and the solid lines are the fit.

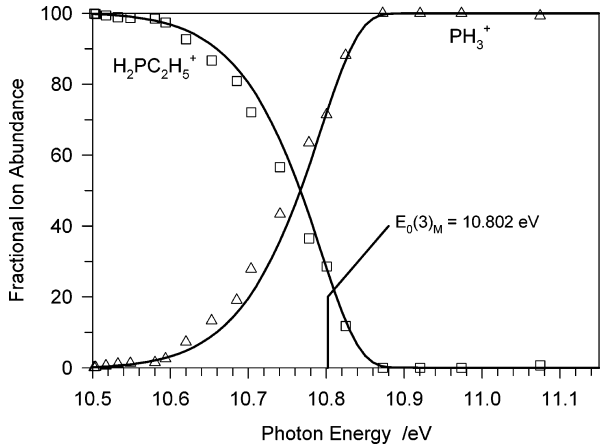

Figure 9. Breakdown diagram for monoethylphosphine from 10.5 to 11.1 eV. The open points are the experimentally determined fractional ion abundances, and the solid lines are the fit.

The first C_2H_4 loss channel in $HP(C_2H_5)_2$ produces the monoethylphosphine ion, $H_2PC_2H_5^+$, illustrated as follows:

$$HP(C_2H_5)_2 + h\nu \rightarrow HP(C_2H_5)_2^+ \rightarrow H_2PC_2H_5^+ + C_2H_4 \quad (8)$$

where the first step represents the adiabatic ionization energy, and the second, the energy difference between $HP(C_2H_5)_2^+$ and $H_2PC_2H_5^+$. This energy difference has already been established from the $P(C_2H_5)_3$ measurements, as has the transition state for C_2H_4 loss, so that the $k(E)$ curve must be the same. The only adjustable parameter is the adiabatic ionization energy of $HP(C_2H_5)_2$, which serves to establish the total energy scale. The best fit to the data is achieved with an adiabatic ionization energy of 7.870 ± 0.013 eV, resulting in a dissociation onset, $E_0(2)_D$, of 9.568 ± 0.015 eV.

One of the major assumptions in modeling sequential unimolecular dissociations is that the internal energy of the molecular ion is redistributed statistically between the daughter ion and neutral fragment. It has been shown by Sztáray and Baer[14] that the energy partitioning can be modeled precisely and the confidence and the validity of this model is further enhanced by its successful application to several molecules.[6,14,15] Here, a more rigid check can be employed because two sets of dissociation reactions differ only by the internal energy distribution of the dissociating species. Figure 6 illustrates the difference. On the right-hand side (Figure 6b) is the internal energy distribution of the energy selected $HP(C_2H_5)_2^+$ ions. This narrow energy distribution, with a full width at half-maximum (fwhm) of 0.2 eV, can be compared to the same ion's energy distribution obtained from the first dissociation of $P(C_2H_5)_3^+$, as shown in Figure 6a, with a width of 1 eV. The excess energy above the dissociation limit for $P(C_2H_5)_3^+$ is partitioned between the internal energy of the C_2H_4 neutral ligand plus two degrees of relative translation energy and the internal energy of $HP(C_2H_5)_2^+$. (We use two degrees of freedom for the translations as is done in phase space theory.) Other than the internal energy distribution, the two reactions are the same, so they must be modeled using the same $k(E)$ curve.

The second C_2H_4 loss in $HP(C_2H_5)_2^+$ is modeled in the same manner as that described above for the second onset in the triethylphosphine reaction. The E_0 and the five transition-state frequencies were adjusted until the best fit was obtained, resulting in $k(E)$ curve 3 in Figure 5. The dissociation onset, $E_0(3)_D$, was determined to be 11.870 ± 0.019 eV. The energy difference between $H_2PC_2H_5^+$ and PH_3^+ is 2.302 ± 0.025 eV, given by the difference between the two measured E_0's.

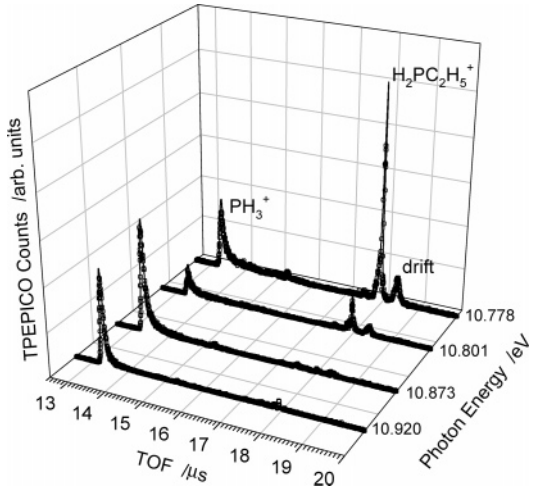

Figure 10. Selected time-of-flight (TOF) distributions for the monoethylphosphine ion recorded using the linear TOF mass spectrometer. The points are experimental TOF distributions, and the solid lines are the fit.

The activation entropy, $\Delta S^{\ddagger}_{600K}$, for the final ethene loss channel is 76.0 J/(K mol), which is indicative of a very loose transition state. When compared to the first two ethene loss channels, the activation entropies increase from −10.1 J K^{-1} mol^{-1} for the first, 2.3 J K^{-1} mol^{-1} for the second, and now 76.0 J K^{-1} mol^{-1} for the third ethene loss. This trend will be discussed later.

Monoethyl Phosphine. The breakdown diagram of monoethylphosphine, $H_2PC_2H_5$, is presented in Figure 9, and selected TOF distributions are given in Figure 10. Since the ion loses 40% of its mass upon dissociation, the experiment was also done on the LinTOF. The sharp symmetric peak at 17.8 μs is the parent ion, and the asymmetric peak that ranges from 13.1 to 14.2 μs is the PH_3^+. The slightly broadened drift peak is present at 18.2 μs.

The onset for this C_2H_4 loss channel is the same as the second C_2H_4 loss channel in diethylphosphine; therefore, $k(E)$ curve 3 is used to model this reaction. The only adjustable parameter is the adiabatic ionization energy which serves to set the total energy scale. The best fit, resulting in an $E_0(3)_M$ of 10.802 ± 0.025 eV, is achieved with an optimized adiabatic ionization energy of 8.500 ± 0.025 eV. The determined E_0's are summarized in Table 3.

In estimating errors for the derived dissociation onsets, some of the parameters were varied in order to obtain an overall best

TABLE 2: Calculated Harmonic Vibrational Frequencies of Relevant Species at the B3LYP/6-311+G Level of Theory**

species	unscaled harmonic frequencies
$P(C_2H_5)_3$	52.1, 71.9, 85.3, 144.7, 161.2, 190.5, 231.2, 251.8, 264.2, 295.1, 346.5, 409.0, 591.9, 646.3, 651.7, 722.7, 755.9, 772.8, 981.7, 982.3, 984.3, 989.3, 995.3, 1021.4, 1053.4, 1059.3, 1066.9, 1260.2, 1267.2, 1277.2, 1280.9, 1287.4, 1297.0, 1411.4, 1412.0, 1414.7, 1463.7, 1464.6, 1471.4, 1497.6, 1499.8, 1501.1, 1504.1, 1504.5, 1509.9, 3015.6, 3017.3, 3022.1, 3023.0, 3023.9, 3027.4, 3052.8, 3056.1, 3056.4, 3079.1, 3079.9, 3080.8, 3089.4, 3091.9, 3099.3
$P(C_2H_5)_3^+$	43.6, 66.3, 70.5, 130.8, 140.6, 169.1, 229.5, 235.5, 255.6, 289.3, 309.3, 376.1, 585.0, 677.3, 685.9, 725.9, 740.8, 771.0, 970.3, 974.9, 979.6, 984.4, 989.1, 1024.0, 1061.0, 1068.7, 1076.0, 1242.2, 1248.3, 1267.4, 1272.4, 1289.9, 1303.3, 1423.4, 1429.3, 1430.0, 1433.0, 1433.4, 1442.4, 1496.7, 1498.7, 1499.2, 1503.1, 1504.7, 1505.2, 2996.7, 3001.1, 3020.9, 3051.5, 3051.7, 3055.0, 3072.7, 3081.3, 3084.7, 3122.8, 3122.8, 3125.0, 3126.1, 3126.8, 3131.6
$HP(C_2H_5)_2$	64.7, 79.3, 158.4, 225.8, 242.9, 280.1, 363.6, 611.6, 645.1, 692.1, 717.6, 832.1, 866.6, 983.0, 988.1, 1017.8, 1060.2, 1070.6, 1076.0, 1271.4, 1278.1, 1289.5, 1295.2, 1409.7, 1415.0, 1462.5, 1473.8, 1497.1, 1500.1, 1502.4, 1504.1, 2338.2, 3019.9, 3022.3, 3023.8, 3027.7, 3054.8, 3067.4, 3076.0, 3081.3, 3092.5, 3096.7
$HP(C_2H_5)_2^+$	54.9, 59.0, 110.1, 215.7, 220.2, 290.0, 303.1, 496.6, 658.4, 658.9, 698.8, 770.9, 862.8, 965.9, 969.9, 984.2, 1051.9, 1066.2, 1079.1, 1231.5, 1254.8, 1281.6, 1292.3, 1420.6, 1428.3, 1428.5, 1430.2, 1495.1, 1495.7, 1497.7, 1498.0, 2463.6, 2990.0, 2999.1, 3051.1, 3051.1, 3080.1, 3082.7, 3123.2, 3123.3, 3128.3, 3128.3
$H_2PC_2H_5$	163.7, 232.1, 282.8, 629.1, 698.7, 813.7, 842.7, 988.3, 1060.1, 1085.8, 1114.5, 1273.4, 1289.8, 1417.0, 1478.2, 1500.9, 1504.9, 2367.2, 2373.0, 3023.9, 3039.2, 3074.2, 3085.7, 3097.9
$H_2PC_2H_5^+$	148.8, 223.6, 263.9, 541.9, 605.6, 693.9, 771.6, 963.0, 1022.1, 1067.6, 1082.9, 1232.5, 1284.7, 1406.5, 1429.5, 1493.2, 1496.2, 2468.4, 2513.2, 2964.8, 3053.2, 3079.5, 3125.8, 3132.4
C_2H_4	771.8, 882.7, 896.9, 1000.4, 1224.0, 1329.3, 1423.2, 1585.9, 3249.1, 3259.6, 3354.3, 3379.2
$TS[HP(C_2H_5)_2\cdots C_2H_4]^+$	54,[a] 69,[a] 80,[a] 85,[a] 185.7, 202.3, 244.4, 276.3, 308.0, 328.9, 384.4, 459.0, 637.2, 666.3, 709.1, 721.7, 768.9, 770.0, 954.6, 963.2, 975.7, 981.1, 1000.8, 1001.3, 1041.1, 1050.3, 1075.7, 1103.0, 1194.8, 1213.3, 1253.9, 1269.0, 1276.9, 1298.4, 1426.9, 1428.1, 1436.0, 1441.5, 1450.6, 1463.2, 1498.1, 1498.9, 1504.1, 1505.5, 1675.6, 3027.2, 3030.7, 3047.3, 3047.4, 3080.6, 3084.1, 3090.2, 3117.5, 3117.8, 3118.1, 3120.2, 3120.2, 3144.0, 3226.7
$TS[H_2PC_2H_5\cdots C_2H_4]^+$	41,[a] 48,[a] 74,[a] 158,[a] 287.1, 417.0, 455.3, 587.4, 649.3, 707.6, 747.8, 809.9, 852.2, 970.8, 973.4, 990.2, 1020.9, 1042.2, 1076.0, 1127.5, 1185.0, 1218.1, 1253.2, 1268.7, 1427.4, 1433.5, 1440.8, 1468.5, 1494.9, 1498.3, 1725.8, 2483.8, 3025.2, 3047.8, 3083.9, 3091.7, 3117.5, 3121.6, 3122.2, 3155.8, 3232.6
$TS[H_3P\cdots C_2H_4]^+$	15[a], 25[a], 30[a], 40[a], 678.2, 738.4, 809.2, 975.3, 1000.2, 1033.8, 1050.1, 1116.7, 1195.6, 1219.5, 1437.4, 1466.3, 1714.9, 2348.0, 2507.5, 3093.4, 3116.8, 3157.1, 3230.3
$TS[H_2C{=}P(C_2H_5)_2\cdots CH_3]^+$	10,[a] 27,[a] 45,[a] 89,[a] 100.0, 193.9, 218.3, 233.6, 263.7, 287.7, 346.8, 375.5, 587.3, 679.8, 684.6, 728.7, 739.1, 771.4, 881.6, 968.2, 978.8, 981.4, 987.8, 1022.3, 1043.5, 1048.6, 1072.7, 1156.5, 1247.4, 1261.5, 1277.5, 1288.0, 1306.3, 1333.7, 1426.4, 1427.6, 1436.7, 1439.0, 1475.1, 1476.2, 1496.1, 1498.3, 1500.4, 1502.2, 2969.0, 2996.1, 3000.7, 3049.4, 3049.6, 3058.2, 3070.9, 3079.3, 3120.2, 3120.7, 3122.4, 3123.6,3145.4, 3148.8, 3167.4

[a] Denotes optimized transition-state frequency from the analysis of the experimental data.

fit for the data from all three molecules. In summary, the adjusted variables were the energies of the three starting molecules as well as the ion energies for the di- and monoethylphosphine and three transition-state vibrational frequencies. (We ignore the CH_3 loss, which is a minor channel that does not affect the analysis of the sequential loss reactions.) With these eight parameters, it was possible to fit absolute rates and relative rates at high energies for five reactions, two each from the tri- and di-, and one from the monoethylphosphine. Because each of these reactions requires two parameters, E_0 and the transition-state frequencies, the number of unknowns is 10. Thus, our six variables have successfully modeled a 10 parameter data set.

Thermochemistry

The measured dissociative photoionization onsets permit us now to establish the heats of formation of all three neutral ethylphosphines and their ions by anchoring the energy scale to the $\Delta_f H°_{0K}[PH_3^+]$ of 966.2 ± 2.0 kJ/mol. The latter value is determined from the $\Delta_f H°_{298K}[PH_3]$ of 5.4 ± 1.7 kJ/mol, based on the heats of explosive decomposition of Gunn and Green[48] and an experimental adiabatic ionization energy of 9.869 ± 0.002 eV from Berkowitz et al.[49] Our own W1U calculation of the adiabatic ionization energy of 9.882 eV supports the experimental measurement to within 1.3 kJ/mol. The thermochemistry also relies on the well-known $\Delta_f H°_{0K}[C_2H_4]$ of 61.05 ± 0.4 kJ/mol, listed in several of the major compilations.[10,50,51] The resulting thermochemistry, which was obtained using eq 1, is summarized in Table 4. Figure 11 summarizes the 0 K thermochemistry and the measured ionization and dissociative ionization onsets.

TABLE 3: Dissociation Onsets for the C_2H_4 Loss Channels

reaction	TPEPICO E_0 (eV)	lit. AE (eV)
$P(C_2H_5)_3 \rightarrow HP(C_2H_5)_2^+ + C_2H_4$	9.041 ± 0.014[a]	10.7 ± 0.3[c]
$P(C_2H_5)_3 \rightarrow H_2PC_2H_5^+ + 2\ C_2H_4$	10.740 ± 0.022[a]	12.7 ± 0.2[c]
		12.3 ± 0.3[d]
$P(C_2H_5)_3 \rightarrow PH_3^+ + 3\ C_2H_4$	13.020 ± 0.043[b]	14.7 ± 0.2[c]
		14.2 ± 0.3[d]
$HP(C_2H_5)_2 \rightarrow H_2PC_2H_5^+ + C_2H_4$	9.568 ± 0.015[a]	10.9 ± 0.3[d]
$HP(C_2H_5)_2 \rightarrow PH_3^+ + 2\ C_2H_4$	11.870 ± 0.019[a]	12.8 ± 0.3[d]
$H_2PC_2H_5 \rightarrow PH_3^+ + C_2H_4$	10.802 ± 0.025[a]	11.2 ± 0.2[c]

[a] Measured TPEPICO onset. [b] Calculated onset from known heats of formation of PH_3^+, C_2H_4, and $P(C_2H_5)_3$. [c] Wada and Kiser.[3] [d] Bogolyubov, Grishen et al.[4]

Discussion

The derived thermochemistry would be affected if a reverse energy barrier were present in the ethene loss reactions. Because such a barrier is quite plausible for a reaction that involves a hydrogen-transfer step, we need to consider this possibility. As a starting point, the structures and energies for several structures along the reaction path were calculated at the B3LYP/6-311+G** level of theory. In all three ions, a tight transition state corresponding to a hydrogen transfer from the carbon to phosphorus atom separated the starting structure and a stable intermediate, which is a four-coordinated central phosphorus atom where the positive charge is located. At the DFT level, the energy of this intermediate relative to the dissociated products was −150, −110, and −100 kJ/mol for the mono- di-, and triethylphosphine ions, respectively. The hydrogen-transfer barrier was found to be 10 and 4 kJ/mol *below* the dissociation product energies for the case of the mono- and diethylphosphine

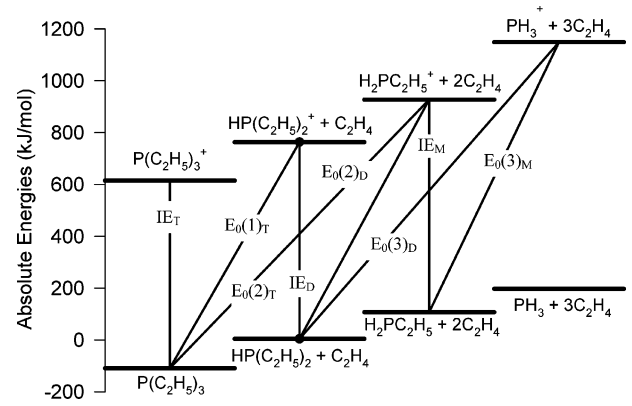

Figure 11. Summary of the derived heats of formation for the ethylphosphine series. The solid lines represent the five measured dissociation onsets and the adiabatic ionization energies.

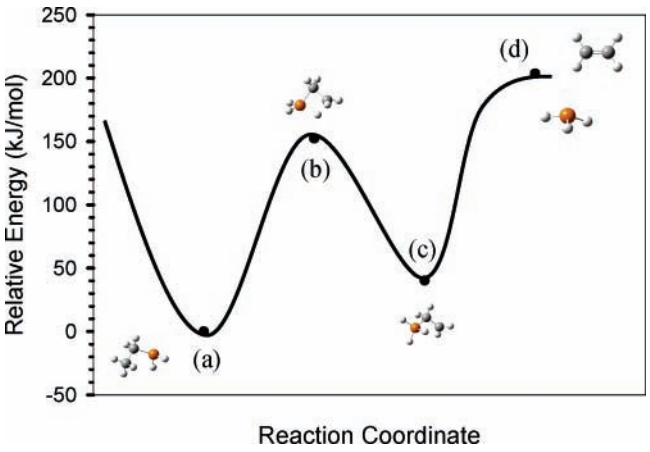

Figure 12. Schematic potential energy diagram for the ethene loss reaction from monoethylphosphine. The points labeled a−d have been calculated at the CCSD(T)/cc-pVTZ//B3LYP/6-311++G** level of theory. The curve has been added to guide the eye.

ions. However, for the case of the triethylphosphine, the barrier was located 5 kJ/mol *above* the energy of the dissociated products. To verify these barriers, we also carried out higher level calculations on these reactions. For the $H_2P(C_2H_5)$ reaction at the CCSD(T)/cc-pVTZ//B3LYP/6-311+G** level, the transition-state energy decreased to 50 kJ/mol *below* the onset for the production of PH_3^+ and C_2H_4. The results are summarized in Figure 12, where points a−d are the coupled-cluster calculated values and the line is present to guide the eye. We conclude that the monoethylphosphine ion (a) rearranges to a stable intermediate (c) by passing through the tight transition state (b). The stable intermediate (c) has three hydrogens and the ethene bound to the phosphine atom. From (c) the ion can dissociate via a loose transition state (not shown) to the products (d). This picture agrees with the experimental results in that the third ethene loss reaction is modeled nicely without taking a reverse barrier into account, yielding an activation entropy of 76 J/(K mol), which is consistent with a loose transition state and barrierless dissociation.

Calculations at the coupled cluster level of theory for the tri- and diethylphosphine were attempted; however, the transition states, analogous to (b) in Figure 12, did not converge. As a result, we do not know for certain whether these barriers would also descend with higher level calculations. However, based on the activation entropies and the agreement between the experimental and calculated thermochemistry, we conclude that the H atom transfer barriers in the case of the di- and triethylphosphines are very close to the dissociation limit. This would account for the negative activation entropy in the triethylphosphine case. It is quite likely that the H atom tunnels through the isomerization barrier. But, because our rates are measured well above the dissociation limit in the triethylphosphine case, we are not sensitive to tunneling. For diethylphosphine, the influence of the first transition state is not as drastic as in the case of triethylphosphine, which is reflected in the activation entropy that lies between the two others.

The derived heats of formation for the three alkylphosphines in Table 4 are compared to calculated values using the following isodesmic reactions.

$$P(C_2H_5)_3 + CH_4 + C_2H_6 \rightarrow P(CH_3)_3 + 2C_3H_8 \quad (9)$$

$$3HP(C_2H_5)_2 + 6CH_4 \rightarrow PH_3 + 2P(CH_3)_3 + 6C_2H_6 \quad (10)$$

$$3H_2PC_2H_5 + 3CH_4 \rightarrow 2PH_3 + P(CH_3)_3 + 3C_2H_6 \quad (11)$$

The heats of reaction were calculated at the G2 and G3 levels of theory, and the average of the two methods was used in conjunction with the established values of the alkanes, PH_3 and $P(CH_3)_3$, listed in Table 5, yielding 298 K heats of formation for $P(C_2H_5)_3$, $HP(C_2H_5)_2$, and $H_2PC_2H_5$ of −145.4, − 88.7, and −38.7 kJ/mol respectively, in good agreement with the experimental results. The least well-established value of the ancillary

TABLE 4: Heats of Formation at 298 and 0 K for Tri-, Di-, and Monoethylphosphine Ions and Neutrals

	TPEPICO experiment (kJ/mol)		lit. and theory (kJ/mol)		
species	$\Delta_f H°_{298K}$	$\Delta_f H°_{0K}$	$\Delta_f H°_{298K}$	$\Delta_f H°_{0K}$	$H_{298K} - H_{0K}$[e]
$P(C_2H_5)_3$	−152.7 ± 2.8	−109.0 ± 2.8	−225[a]	−101.8[b]	31.5
			−145.4[b]		
			−159[c]		
			−150.0 ± 7.0[d]		
$P(C_2H_5)_3^+$	571.6 ± 4.0	614.7 ± 4.0	561[a]	−	32.1
$HP(C_2H_5)_2$	−89.6 ± 2.1	−56.7 ± 2.1	−102[a]	−55.9[b]	23.3
			−88.7[b]		
			−88.4[d]		
$HP(C_2H_5)_2^+$	669.9 ± 2.5	702.3 ± 2.5	736[a]	−	23.7
			820[c]		
$H_2PC_2H_5$	−36.5 ± 1.5	−15.0 ± 1.5	−50.2[c]	−17.2[b]	15.6
			−38.7[b]		
			−36.0[d]		
$H_2PC_2H_5^+$	784.0 ± 1.9	805.2 ± 1.9	962.3[c]	−	16.1

[a] Estimate in Lias et al.[10] [b] Isodesmic reactions as described in paper. [c] These values from Wada and Kiser.[3] are severely outdated and are only included for completeness. [d] Calculated using the G3X method from Dorofeeva and Moiseeva.[12] [e] Calculated using harmonic vibrational frequencies from DFT calculations described in the text.

TABLE 5: Ancillary Thermochemical Data

species	$\Delta_f H°_{298K}$ (kJ/mol)	$\Delta_f H°_{0K}$ (kJ/mol)	$H_{298K} - H_{0K}$[d]
PH_3	5.02 ± 1.00[a]	13.97 ± 1.00[a]	10.1
$P(CH_3)_3$	-101 ± 5.0[b]	-76.3 ± 5.0[b]	20.4
C_2H_4	52.5 ± 0.4[c]	61.05 ± 0.4[d]	10.5
C_2H_6	-83.8 ± 0.4[c]	-68.0 ± 0.4[d]	11.7
C_3H_8	-104.7 ± 0.5[c]	-82.2 ± 0.5[d]	14.5

[a] Gunn and Green.[48] [b] Lias et al.[10] [c] Pedley.[51] [d] Calculated using harmonic vibrational frequencies.

species is the trimethylphosphine with a quoted error of 5 kJ/mol. The largest disagreement between the calculated and experimental values is for the case of the triethylphosphine, in which the calculated value is about 7 kJ/mol (70 meV) higher than the experimental value, a value outside our experimental uncertainty. We cannot attribute this discrepancy to the uncertainty in the $P(CH_3)_3$ heat of formation because the error does not appear in the di- and monoethylphosphine determinations.

Independent verification of the neutral heats of formation comes from the work of Dorofeeva and Moiseeva,[12] who used a series of isodesmic reactions computed with the G3X of theory. They report a 298 K heat of formation of -150.0 ± 7.0 kJ/mol for triethylphosphine, which is in excellent agreement with our measured and calculated values. Additionally, using the group additivity values provided by Dorofeeva and Moiseeva,[12] the 298 K heats of formation of -88.4 and -36.0 kJ/mol are obtained for $HP(C_2H_5)_2$ and $H_2P(C_2H_5)$, respectively. These are in excellent agreement with our measured, -89.6 and -36.5 kJ/mol, and calculated, -88.7 and -38.7 kJ/mol, values as well.

So far, we note that our experimentally derived energies are in good agreement with both sets of calculated ones and it would appear that these ethylphosphine heats of formation are now reliably established. However, the implication for the ionization energies is a bit more problematic. Aside from the heat of formation of the $P(C_2H_5)_3^+$, all of the thermochemistry in Table 3 was obtained from the dissociative photoionization experiments. Because we have determined both the neutral and the ion energies, we know directly the adiabatic ionization energies of the diethyl- and monoethylphosphines, which can be compared to those obtained from the ab initio calculations, and those derived from the photoelectron spectra in Figures 1 and 2.

The arrows in Figures 1 and 2 point to the experimental ionization energies for the triethyl- and monoethylphosphines. It is evident that the TPEPICO-derived adiabatic IE's are considerably below what might be called the phenomenological adiabatic IE's. But, as already pointed out, the large change in the geometry upon ionization, from an out of planar PC_3 angle of 30° to 15° and the low vibrational frequency associated with this umbrella mode, makes the experimental adiabatic IE difficult to establish. The calculated IE's listed in Table 1 do not offer much resolution. They agree with the lower TPEPICO value for the case of the triethylphosphine but agree better with the phenomenological IE of the monoethylphosphine. Support for the 7.50 eV value of the triethylphosphine IE comes also from the study of Gengeliczki et al.[6] who measured the collision-induced dissociation onsets for $CoP(C_2H_5)_3^+$ ion, which resulted in the production of the $P(C_2H_5)_3^+$ ion at a collision energy some 0.38 eV below that of the Co^+ ion. With the assumption that this energy difference is the difference in the ionization energies of Co (7.881 eV [6,52]) and $P(C_2H_5)_3$, they concluded that the latter's adiabatic IE is 7.50 ± 0.30 eV, which is in perfect agreement with our TPEPICO result. In support for our low IE value for the monoethylphosphine, we note that the 8.50 eV TPEPICO value is shifted about equally to lower energy from the phenomenological adiabatic ionization energy as it is in the trimethylphosphine case.

Conclusion

We have used three $k(E)$ curves to model five sets of experimental data on C_2H_4 loss reactions in a series of energy selected ethylphosphine ions and have determined their dissociation onsets. Coupling these measured onsets with reliable ancillary thermochemical values, new heats of formation for several ions and neutrals have been determined. These new accurate and reliable values can be applied to phosphine-containing systems such as derivatives of transition metal carbonyls to help solidify the thermochemistry of those systems. The redundancy has provided a valuable check of the calculation of the internal energy distribution as well as the energy partitioning between the ion and the neutral fragment.

Acknowledgment. We gratefully thank the Department of Energy and the International Office of the National Science Foundation for the support of this work. J.P.K. thanks the Center for International Studies at the University of North Carolina for their gracious support to allow much of this work to be done in Budapest, Hungary. The cooperation between the U.S. and Hungarian groups was also supported by a joint MTA-OTKA-NSF grant. We are also grateful to the Országos Tudományos Kutatási Alap (Grant Nos. F61153 and T032489).

References and Notes

(1) Serron, S.; Huang, J.; Nolan, S. P. *Organometallics* **1998**, *17*, 534−539.
(2) Tanaka, H.; Hara, Y.; Watanabe, E.; Wada, K.; Onoda, T. *J. Organomet. Chem.* **1986**, *312*, C71−C74.
(3) Wada, Y.; Kiser, R. W. *J. Phys. Chem.* **1964**, *68*, 2290.
(4) Bogolyubov, G. M.; Grishin, N. N.; Petrov, A. A. *Zh. Obsch. Khim.* **1969**, *39*, 1808−1816.
(5) Yarbrough, L. W.; Hall, M. B. *Inorg. Chem.* **1978**, *17*, 2269−2275.
(6) Gengeliczki, Z.; Sztáray, B.; Baer, T.; Iceman, C.; Armentrout, P. B. *J. Am. Chem. Soc.* **2005**, *127*, 9393−9402.
(7) Valentine, D. H., Jr.; Hillhouse, J. H. *Synthesis* **2003**, *16*, 2437−2460.
(8) Valentine, D. H., Jr.; Hillhouse, J. H. *Synthesis* **2003**, *3*, 317−334.
(9) Bodi, A.; Kercher, J. P.; Baer, T.; Sztáray, B. *J. Phys. Chem. B* **2005**, *109*, 8393−8399.
(10) Lias, S. G.; Bartmess, J. E.; Liebman, J. F.; Holmes, J. L.; Levin, R. D.; Mallard, W. G. Gas-Phase Ion and Neutral Thermochemistry. *Journal of Physical and Chemical Reference Data*, Vol. 17, Suppl. 1; NSRDS, U. S. Government Printing Office: Washington, DC, 1988.
(11) Cox, J. D.; Pilcher, G. *Thermochemistry of Organic and Organometallic Compounds*; Academic Press: London, 1970.
(12) Dorofeeva, O. V.; Moiseeva, N. F. *J. Phys. Chem. A* **2006**, *110*, 8925−8932.
(13) Baer, T.; Sztáray, B.; Kercher, J. P.; Lago, A. F.; Bodi, A.; Scull, C.; Palathinkal, D. *Phys. Chem. Chem. Phys.* **2005**, *7*, 1507−1513.
(14) Sztáray, B.; Baer, T. *J. Phys. Chem. A* **2002**, *106*, 8046−8053.
(15) Sztáray, B.; Baer, T. *J. Am. Chem. Soc.* **2000**, *122*, 9219−9226.
(16) Baer, T.; Mazyar, O. A.; Keister, J. W.; Mayer, P. M. *Ber. Bunsen-Ges. Phys. Chem.* **1997**, *101*, 478−483.
(17) Baer, T.; Brand, W. A.; Bunn, T. L.; Butler, J. J. *Faraday Discuss.* **1983**, *75*, 45−55.
(18) Duffy, L. M.; Keister, J. W.; Baer, T. *J. Phys. Chem.* **1995**, *99*, 17862−17871.
(19) Khundkar, L. R.; Marcus, R. A.; Zewail, A. H. *J. Phys. Chem.* **1983**, *87*, 2473−2476.
(20) Mazyar, O. A.; Mayer, P. M.; Baer, T. *Int. J. Mass Spectrom. Ion Processes* **1997**, *167/168*, 389−402.
(21) Mazyar, O. A.; Baer, T. *J. Phys. Chem. A* **1998**, *102*, 1682−1690.
(22) Mazyar, O. A.; Baer, T. *J. Phys. Chem. A* **1999**, *103*, 1221−1227.
(23) Chupka, W. A. *J. Chem. Phys.* **1959**, *30*, 191−211.
(24) Huang, F. S.; Dunbar, R. C. *J. Am. Chem. Soc.* **1990**, *112*, 8167−8169.
(25) Lifshitz, C. *Mass Spectrom. Rev.* **1982**, *1*, 309−348.
(26) Kercher, J. P.; Sztáray, B.; Baer, T. *Int. J. Mass Spectrom.* **2006**, *249*, 403−411.
(27) Lifshitz, C. *J. Phys. Chem.* **1982**, *86*, 606−612.

(28) Lifshitz, C.; Gotchiguian, P.; Roller, R. *Chem. Phys. Lett.* **1983**, *95*, 106−108.
(29) Troe, J.; Ushakov, V. G.; Viggiano, A. A. *J. Phys. Chem. A* **2006**, *110*, 1491−1499.
(30) Baer, T.; Hase, W. L. *Unimolecular Reaction Dynamics: Theory and Experiments*; Oxford University Press: New York, 1996.
(31) Marcus, R. A.; Rice, O. K. *J. Phys. Colloid Chem.* **1951**, *55*, 894−908.
(32) Fogleman, E. A.; Koizumi, H.; Kercher, J. P.; Sztáray, B.; Baer, T. *J. Phys. Chem. A* **2004**, *108*, 5288−5294.
(33) Kercher, J. P.; Fogleman, E. A.; Koizumi, H.; Sztáray, B.; Baer, T. *J. Phys. Chem. A* **2005**, *109*, 939−946.
(34) Lago, A. F.; Kercher, J. P.; Bodi, A.; Sztáray, B.; Miller, B. E.; Wurzelmann, D.; Baer, T. *J. Phys. Chem. A* **2005**, *109*, 1802−1809.
(35) Sztáray, B.; Baer, T. *Rev. Sci. Instrum.* **2003**, *74*, 3763−3768.
(36) Sztáray, B.; Szepes, L.; Baer, T. *J. Phys. Chem. A* **2003**, *107*, 9486−9490.
(37) Frisch, M. J.; Trucks, G. W.; Schlegel, H. B.; Scuseria, G. E.; Robb, M. A.; Cheeseman, J. R.; Montgomery, J. A.; Vreven, T.; Kudin, K. N.; Burant, J. C.; Millam, J. M.; Iyengar, S. S.; Tomasi, J.; Barone, V.; Mennucci, B.; Cossi, M.; Scalmani, G.; Rega, N.; Petersson, G. A.; Nakatsuji, H.; Hada, M.; Ehara, M.; Toyota, K.; Fukuda, R.; Hasegawa, J; Ishida, M.; Nakajima, T.; Honda, Y.; Kitao, O.; Nakai, H.; Klene, M.; Li, X.; Knox, J. E.; Hratchian, H. P.; Cross, J. B.; Adamo, C.; Jaramillo, J.; Gomperts, R.; Stratmann, F.; Yazyev, O.; Austin, A. J.; Cammi, R.; Pomelli, C.; Ochterski, J. W.; Ayala, P. Y.; Morokuma, K.; Voth, G. A.; Salvador, P.; Dannenberg, J. J.; Zakrzewski, V. G.; Dapprich, S.; Daniels, A. D.; Strain, M. C.; Farkas, Ö.; Malick, D. K.; Rabuck, A. D.; Raghavachari, K.; Foresman, J. B.; Ortiz, J. V.; Cui, Q.; Baboul, A. G.; Clifford, S.; Cioslowski, J.; Stefanov, B. B.; Liu, G.; Liashenko, A.; Piskorz, P.; Komáromi, I.; Martin, R. L.; Fox, D. J.; Keith, T.; Al-Laham, M. A.; Peng, C. Y.; Nanayakkara, A.; Challacombe, M.; Gill, P. M. W.; Johnson, B.; Chen, W.; Wong, M. W.; Gonzalez, C.; Pople, J. A. *Gaussian 03*, Revision C.02; Gaussian, Inc.: Pittsburgh, PA, 2004.
(38) Becke, A. D. *J. Chem. Phys.* **1993**, *98*, 5648−5652.
(39) Lee, C.; Yang, W.; Parr, R. G. *Phys. Rev.* **1988**, *B37*, 785−789.
(40) Peng, C.; Ayala, P. Y.; Schlegel, H. B.; Frisch, M. J. *J. Comput. Chem.* **1996**, *17*, 49−56.
(41) Curtiss, L. A.; Raghavachari, K.; Redfern, P. C.; Rassolov, V.; Pople, J. A. *J. Chem. Phys* **1998**, *109*, 7764−7776.
(42) Montgomery, J. A., Jr.; Frisch, M. J.; Ochterski, J. W.; Petersson, G. A. *J. Chem. Phys.* **2006**, ***110***, 2822−2827.
(43) Curtiss, L. A.; Raghavachari, K.; Trucks, G. W.; Pople, J. A. *J. Chem. Phys.* **1991**, *94*, 7221−7230.
(44) Curtiss, L. A.; Redfern, P. C.; Smith, B. J.; Radom, L. *J. Chem. Phys.* **1996**, *104*, 5148−5152.
(45) Curtiss, L. A.; Raghavachari, K.; Pople, J. A. *J. Chem. Phys.* **1993**, *98*, 1293−1298.
(46) Hampel, C.; Peterson, K. A.; Werner, H.-J. *Chem. Phys. Lett.* **1992**, *190*, 1−12.
(47) Van Hooijdonk, M. C. J. M.; Gerritsen, G.; Brandsma, L. *Phosphorus, Sulfur Silicon Relat Elem.* **2000**, *162*, 39−49.
(48) Gunn, S. R.; Green, L. G. *J. Phys. Chem.* **1961**, *65*, 779−783.
(49) Berkowitz, J.; Curtiss, L. A.; Gibson, S. T.; Greene, J. P.; Hillhouse, G. L.; Pople, J. A. *J. Chem. Phys.* **1986**, *84*, 375−384.
(50) Pedley, J. B.; Naylor, R. D.; Kirby, S. P. *Thermochemical Data of Organic Compounds*; Chapman and Hall: London, 1986.
(51) Pedley, J. B. *Thermochemical Data and Structures of Organic Compounds*; Thermodynamics Research Center: College Station, TX, 1994.
(52) *JANAF Thermochemical Tables*; American Institute of Physics, Inc.: New York, 1986.